

## Article

# Assessment of the Use of Infrared Laser for Dynamic Laser Speckle (DLS) Technique

Ellem W. N. Contado <sup>1</sup>, Moacir Pasqual <sup>2</sup>, Joyce Dória <sup>2</sup> , Rolando J. Gonzalez-Peña <sup>3</sup> , Lionel X. Dupuy <sup>4,5</sup>  and Roberto A. Braga, Jr. <sup>1,\*</sup> 

<sup>1</sup> Departament of Automatica (DAT), Federal University of Lavras (UFLA), Lavras 37.200-000, MG, Brazil

<sup>2</sup> Departament of Agriculture (DAG), Federal University of Lavras (UFLA), Lavras 37.200-000, MG, Brazil

<sup>3</sup> Department of Physiology, Universitat de València, 46010 València, Spain

<sup>4</sup> Ikerbasque, Basque Foundation for Science, 48009 Bilbao, Spain

<sup>5</sup> Department of Conservation of Natural Resources, Neiker, 48160 Derio, Spain

\* Correspondence: robbraga@ufla.br

**Abstract:** Dynamic laser speckle (DLS) analysis is a very sensitive technique to measure biological activity within samples. In agriculture, the technique is applied to monitor seed germination, but external light, water content, and pigments affect the measurements. DLS systems use visible light sources, typically red lasers, which may exacerbate their influences. The main objective of this work is to assess whether infrared (IR) lasers improve the robustness of DLS measurements in seed germination applications. We develop a system where DLS analysis can be performed simultaneously on visible and IR light. Using the system, we quantify how the DLS signal is affected by pigments and scattering. The results show that the use of IR light reduces the variability of the measurements acquired. DLS systems based on IR light appear to be less sensitive to pigments, and the greater penetration of IR light into samples, which is due to reduced scattering, may contribute to the signal collected being correlated to relevant biological processes within the inner tissue. Additionally, water activity provides less influence on the DLS signal when an IR laser is used. These findings support the wider use of IR lasers in DLS-based instruments for applications in biological samples.



**Citation:** Contado, E.W.N.; Pasqual, M.; Dória, J.; Gonzalez-Peña, R.J.; Dupuy, L.X.; Braga, R.A., Jr. Assessment of the Use of Infrared Laser for Dynamic Laser Speckle (DLS) Technique. *Agriculture* **2023**, *13*, 546. <https://doi.org/10.3390/agriculture13030546>

Academic Editor: Massimo Cecchini

Received: 20 December 2022

Revised: 17 February 2023

Accepted: 20 February 2023

Published: 23 February 2023



**Copyright:** © 2023 by the authors. Licensee MDPI, Basel, Switzerland. This article is an open access article distributed under the terms and conditions of the Creative Commons Attribution (CC BY) license (<https://creativecommons.org/licenses/by/4.0/>).

## 1. Introduction

Since the construction of the first laser in 1960 by Theodore H. Maiman, the technique has become central to modern metrology. This has been the case in agriculture [1,2], where remote monitoring of a crop is critical to manage production and yield with precision [3]. Current uses of lasers include chemical-free weeding systems [4] and measurements of photosynthesis through chlorophyll fluorescence [5]. LiDAR (light detection and ranging) is particularly prevalent in agriculture with applications for estimating plant growth and yield [6,7], navigating robots in fields [8], detecting crop damage [9], mapping soil types, and predicting moisture [10].

Interferometry is one broad range of techniques where the laser is used to produce light interference patterns that inform about properties of the object that creates the interference. A classic example is the interferometer of Michelson which can be used to measure distance with a precision of below one micron. Dynamic laser speckle (DLS) analysis exploits the dynamics of the interference patterns to infer about the speed at which a process is taking place within a sample. The phenomenon has been used to monitor processes in non-biological samples, e.g., paint drying [11] and particle size measurement [12]. In biology, DLS analysis has been used to measure superficial blood flow rate in human patients and rats in laboratory experiments [13,14] as well as to monitor a broad range of biological samples in agriculture [15,16]. Applications in agriculture include the assessment of the viability of seeds [17,18], the fungal contamination of seeds [19], the identification of

meristematic regions in roots [20], the monitoring of fruit maturation [21] or water activity in leaves [22], as well as developing diagnostic tools for the early detection of the bruising in fruits [23]. The technique has also been used in animal and human science to assess the aging of meat [24] and to detect the presence of parasites in blood [25]. Those are some examples of the feasibility of using DLS analysis as an alternative tool to follow tiny changes in biological material with the advantages of offering objective judgment; the possibility of automation; in some cases, low cost; and being a non-contact and non-destructive (NDT) technique.

The complexity of light interactions with living tissues has been well-characterized, notably in relation to biomedical applications [26,27]. Light interacts with biological tissues through reflection, transmission, scattering, and absorption, and the proportion of each of these phenomena varies significantly between living samples. Thus, the success of DLS techniques lies on its ability to capture such changes reliably. Micro- or nanoscale biological structures that are not directly resolved by a regular objective or light sensor can still generate an indirect signal through the light interference whose dynamics are related to movements within the tissues. For example, semen mobility was quantified successfully with DLS analysis using images of speckle patterns as a result of the sperm motility, even when the imaging resolution of the optical apparatus was not tailored to monitor a single spermatozoon [28].

The sensitivity of the DLS technique to small changes can also be a limitation. Small variations in the angle of the illumination or the position of the camera (Figure 1) can affect the output of DLS signals [29]. The appearance of the sample can also affect the results significantly; i.e., pigments from leaves or fruits vary during maturation and this is challenging to measure [22]. Similar problems arise from the monitoring of meat quality, where white fat contents within the red tissue can compromise the results of DLS [24]. Finally, water content strongly affects the optical properties at the interface of the sample with the air. Changes in the refractive index are known to induce large variability in the results of DLS analyses, too [30]. Therefore, there is a need for improvement in the DLS technique to circumvent obstacles to reliably measure biological phenomena.

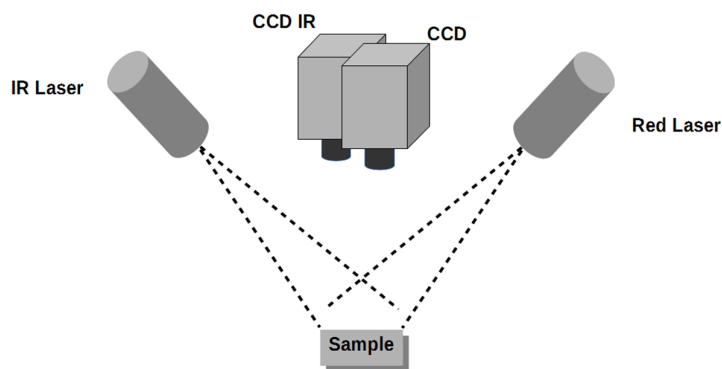


**Figure 1.** Common set-up of illumination and image acquiring with devices dedicated to red and IR (infrared) wavelength.

The wavelength of the laser is an important factor affecting the DLS signal. The choice of a suitable wavelength of the laser source is therefore essential for the successful application of DLS analyses. The selection of the laser source and its wavelength in DLS application is often motivated by practical considerations, such as its availability and its cost. For this reason, red lasers (632–660 nm) have been most used in DLS studies. The choice of the wavelength of the laser light source has rarely been based on the nature of the sample or on the process studied. The use of red lasers to monitor leaf water content, for example, proved to be limited [22]. Chlorophyll absorbs red light, and this led to changes in the DLS signal, which became a function of chlorophyll content [31]. The wavelength of the light source also determines the depth from which a biospeckle laser signal is obtained, and the air–sample interfaces induce an undesirable signal, as was demonstrated in the

case of respiration in processed carrots [32]. The problem can be addressed by filtering the digital signal, but this often leads to loss of information [33].

It is also surprising, considering the importance of scattering at the air/sample interface, that the use of infrared (IR) laser sources for biospeckle laser technique applications remains limited. This may be due to additional costs of IR optical devices and the challenges of working with hazardous light that is not visible. The use of the IR laser in dynamic laser speckle (DLS) analysis has been developed to monitor the drying of paints [34,35]. Pérez et al. [35] showed that IR laser use allows the improvement of the robustness of the technique in the presence of environmental or artificial light when compared to visible red and green lasers. However, such techniques have not been tested much. For example, a 780 nm laser was used to monitor apple activity using a DLS system in order to avoid absorption of the laser beam [36]. Others studies tested IR lasers (780 nm [37], 830 nm [38]) to quantify the chlorophyll content in plants/fruits in comparison to red lasers. In apples, the classification using dynamic laser speckle analysis with a red laser were better than case of an IR laser (780 nm) [37]. In turn, the dynamic laser speckle analysis from of IR laser presented lower variability when monitoring tomato ripening than the dynamic laser speckle analysis using the red laser [38].

Biological samples have many sources of variability, and IR laser sources could improve the robustness of the dynamic laser speckle analyses with potential for reducing sensitivity to pigments and increasing the penetration of light within the sample [31]. To date there have been few studies on the use of IR lasers in DLS approaches [34,35], and none have focused thoroughly on the study of biological samples as we planned to do in this work [36–38]. Therefore, the objective of this study was to test if IR lasers, when compared to visible lasers, can improve the reliability of DLS techniques regarding the pigment content, water activity, and penetration in the sample. We developed a system to monitor the DLS signals from both visible and IR lasers on drying paint with different colours and on seedlings placed within gel substrates with different pigmentation or directly exposed to laser.

## 2. Materials and Methods

### 2.1. Image Acquisition Set-Up

The image acquisition set-up was designed to collect timelapse data of the speckle patterns formed by IR and red laser light scattered from the same sample (Figure 1). For illumination with IR, a 780 nm solid-state laser (PLD1 IZI 50-780, LASERLine, Amparo, Brazil) was used. For illumination with visible light, a 660 nm solid-state laser (IZI 40-660, LASERLine, Amparo, Brazil) was used. Visible and IR scattered light was collected from the same sample by two distinct cameras positioned vertically over the sample and placed about 100 mm apart. The lasers were positioned at a distance of 200 mm from the sample and at an angle of 60°. The two diode lasers and the cameras were 1280 × 1024-pixel mini-microscopes (AM413ZT, Dino-Lite, Torrance, CA, USA) and 1280 × 1024-pixel mini-microscopes (AM4115FKT, Dino-Lite, Torrance, CA, USA) for visible and IR light, respectively. Images were acquired at a resolution of 640 × 480 pixels for image processing. The cameras were chosen to have their highest sensitive value in the range of 660 and 780 nm, and their magnifications were adjusted to ensure the dimensions of the samples in the images were identical. Minor adjustments to the zoom and focus were then made for images to have similar speckle size distributions, as well as the same digital size of the illuminated objects. To correct for the biases introduced by the illumination system, images of brown paper (Paper Kraft, 80 g m<sup>-2</sup>) were acquired by both cameras, and the power output of the lasers was set for both images to have histograms with a similar mean pixel intensity and without saturation of light. The IR laser required 32% more power than the red laser to provide the same intensity of light. These adjustments were kept constant through all assays. All experiments were carried out in the dark.

Images were acquired using the free software Speckle Tool (MHI), version 1.0, UFLA, Lavras, Brazil [39,40]. The acquisition data were achieved at 10 fps and with the magnifi-

cation adjusted to obtain similar speckle patterns in the samples (grain sizes). A total of 128 images were assembled in time to obtain indices for DLS activity.

## 2.2. Testing of Pigment Effects Using Drying Paints

To study the effects of pigments on the nature of the DLS signal, we studied the DLS analysis obtained from two different paints (enamel inks of composition: butyl acetate, ethyl acetate, nitrocellulose, acetyl tributyl citrate, isopropyl alcohol, stearalkonium hectorite, tosylamide/epoxy resin, polyethylene, terephthalate) in red and green colours. The choice of red and green pigmented paints was motivated by the fact that both red and green lasers are used in DLS applications and pigments of both colours exists in plants, e.g., chlorophyll [36–38]. One layer of ink was painted on a side of a glass slide, covering an area of  $1.5 \text{ cm}^2$ . Five replicates were produced for each paint. DLS data on drying ink were acquired during the first five min of drying, when volatilization is most intense and produces strong DLS signals.

## 2.3. Plant Growth

*Zea mays* L. seeds were used in the study, and the crop was located at latitude  $21^\circ 23' 151''$  S, longitude  $44^\circ 99' 482''$  W Gr. and 918 m above sea level in Lavras MG Brazil, Köppen climate classification, Cwa, temperate rainy. The harvesting was in the fall of 2018 when the seeds were used in the assays. The seedlings (*Zea mays* L.) were illuminated two days after germination. The germination paper was imbibed with distilled water and did not contain nutrient solutions. Seeds were placed in a germination paper in a germination chamber with Bio-Oxygen Demand (BOD) at  $30^\circ \text{C}$ . After two days, germinated seeds (seedlings) were taken from the BOD and the paper was opened for 30 min to let the seeds lose the excessive water over them.

Plants were grown in agar gels prepared with potato-dextrose-agar, whose application is common in culture of tissues and DLS analysis of growing roots [20]. A total of 5 g of agar was dissolved in 250 mL of distilled water and heated at  $100^\circ \text{C}$ . To dye the agar, 0.25 mL of black food dye was added to 250 mL of distilled water before 5 g of agar was dissolved and heated at  $100^\circ \text{C}$ . The dye was composed of ethyl alcohol, artificial colours, Red II, Blue I, and Tartrazine Yellow.

## 2.4. Direct Illumination of Maize Seedlings with Red and IR Lasers

The seeds were placed one by one on a brown paper (Paper Kraft,  $80 \text{ g m}^{-2}$ ) and centred in the field of view of the cameras (Figure 2A). The lasers were switched on 30 min before, and the seeds were illuminated once by the red laser beam, and after horizontal rotation, by the IR laser. During each stage of illumination, 128 images were acquired at 10 frames per second (Figure 1).

## 2.5. Effects of Substrate Transmittance on DLS Measurement

The assay used two layers of agar gels introduced into an 80 mL glass test tube (2.5 cm diameter and 20 cm height). The layers of equal size were positioned along the tube (Figure 3A). On one side, the layer consisted of a transparent, no-dye agar gel. On the other side, the layer consisted of dyed agar gel with increased scattering and reduced light transmittance. Maize seedlings were placed at the interface between the two layers of gel so that roots growing in the tube could be imaged through either gel layer that were with and without dye. Observations were made two days after germination. Seeds were placed in the tube over the first layer introduced (no dye) just after the gel solidified (approximately 20 min) with the tube in the horizontal position. The second layer, consisting of dyed gel, was introduced still in a liquid state (with temperature close to ambient) and was allowed to solidify for 20 min (Figure 3A).

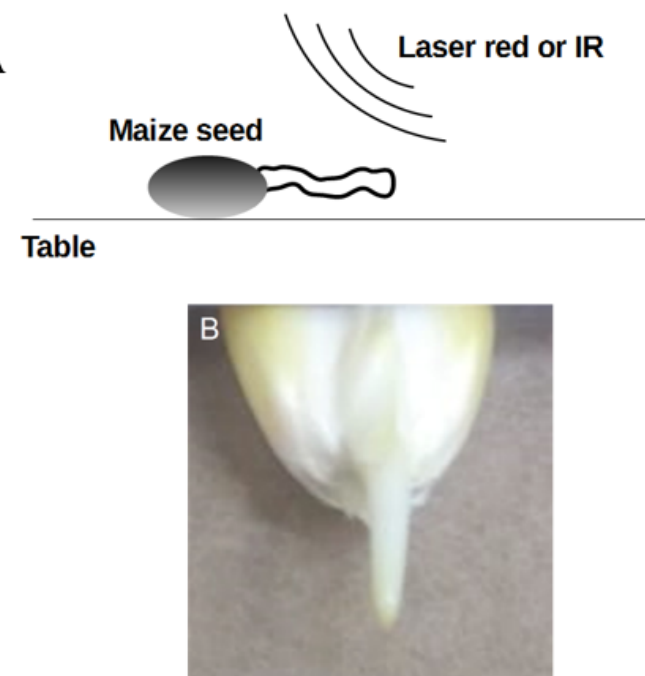


**Figure 2.** Seed imaging system. (A) Disposition of the seed on the table with a dry paper between them indicating the angle of the illumination with the cameras placed perpendicularly to the table and sample; (B) example of image obtained from a maize seed image without laser illumination.

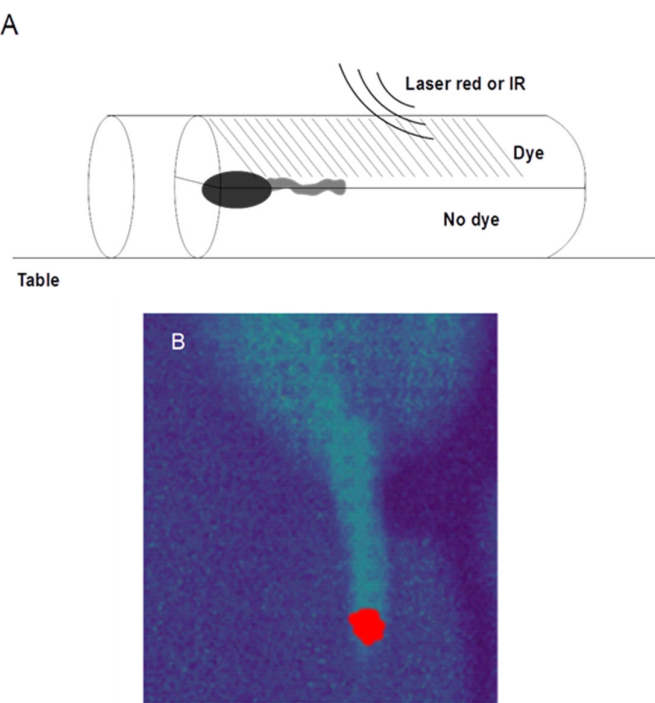


**Figure 3.** Experimental set-up used to study maize seedlings grown in agar. (A) The seedling was grown in a glass tube in between two layers of gel (with and without dye). Cameras were placed 90° over the sample on the table. (B) A total of 100 points (red) were randomly collected at the tip of the root using a Gaussian distribution.

Data were acquired from the illuminated seedlings using red and IR lasers. The tube was rotated to place either the agar gel without dye or the agar gel with dye in front of the cameras. The position of the tube was also adjusted (180° rotation in the imaging place) to ensure that data collected from the red laser were at an identical angle to data collected

from the IR laser. Eight replicates were acquired for each treatment. Images were processed as a whole to obtain the map of activities and in the tip root to get the numerical activity outcome (Figure 3B).

## 2.6. Data Analysis

Images were processed using the package Bio-Speckle Laser Tool Library (BSLTL) [41]. The images acquired were first analysed using their histograms to determine the mean intensity in a region of interest (ROI) of  $640 \times 480$  pixels from only one raw image (speckle pattern) and across different time-points; i.e., the mean intensity was obtained through spatial averaging.

The analysis of the DLS data was carried out graphically and numerically. The graphical outcomes were carried out from the processing of 128 speckle images in time using the standard deviation (SD) algorithm [42].

$$SD = \sqrt{\frac{1}{N} \sum_k^N |I_k - E[I_k]|^2} \quad (1)$$

$N$  is the number of  $k$  images tagged by  $I_k$ , which represents a matrix of grey values, and  $E[.]$  is the temporal mean of the images. The routines are free and can be obtained from BSLTL Project [41].

The numerical analysis of the DLS signals was obtained from the tip of the root. Each DLS dataset had 128 images, where one hundred points were randomly selected at the tip of the root using a Gaussian distribution (red area in the tip of the root). The points were used to create the time history of the speckle pattern (THSP) before the numerical analysis [43].

Numerical analysis of biospeckle images was performed using various indices. We used the absolute value of the differences (AVD) [44].

AVD uses a co-occurrence matrix (COM) derived from the time history of the speckle pattern (THSP), obtained using the randomized Gaussian distribution of points in the tip of the seedling and in the centre of the drying paint, Equation (1). Thus, the THSP records a collection of points of the speckle pattern and their behaviour in time.

$$AVD = \sum_i \sum_j \frac{COM(i,j)}{Normalization} |i - j| \quad (2)$$

where  $i$  and  $j$  are the positions in the matrix COM (co-occurrence matrix) [34] with the normalization representing the summation of all occurrence values per line in the co-occurrence matrix [33]. Therefore, each value of the matrix is divided by the respective summation of the values per line. Therefore, the COM uses the THSP to summarize in its elements the occurrences of some pixels in time, where  $i$  and  $j$  represent grey values in two consecutive moments present in the THSP line, being  $i$  and  $j$  values of grey from 0 to 255.

## 3. Results and Discussions

### 3.1. The Effect of Pigments on DLS Measurements from IR and Red Lasers

Drying paints or coatings are models to characterize the scattering of light, as they are rather a good example of light scatterers. The paint-air interface affects the dynamic of the light scattering and consequently the intensities of the grains in the speckle pattern that are used by the DLS measurements. In this experiment, red paints scattered predominantly the red light, which resulted in a larger quantity of light (signal) collected by the camera (Figure 4), thus giving higher values to the DLS index (AVD) (Figure 5). In the case of drying green paints, red light was predominantly absorbed, which resulted in a low quantity of light acquired from the red laser (Figure 4). The intensity of light returning from the green paint was less than 15 times the intensity that returned from the red pigment when the red laser was used, as expected. In addition, the AVD values obtained using the red laser in

green pigment was the lowest by consequence of the lowest signal (Figure 5). The pigment can compromise the information we expect to obtain when carrying out the DLS analysis. Nevertheless, the light scattered from the green and red paints, collected by the cameras, was 2.2 times the rate in intensity when we used the IR laser (Figure 4).

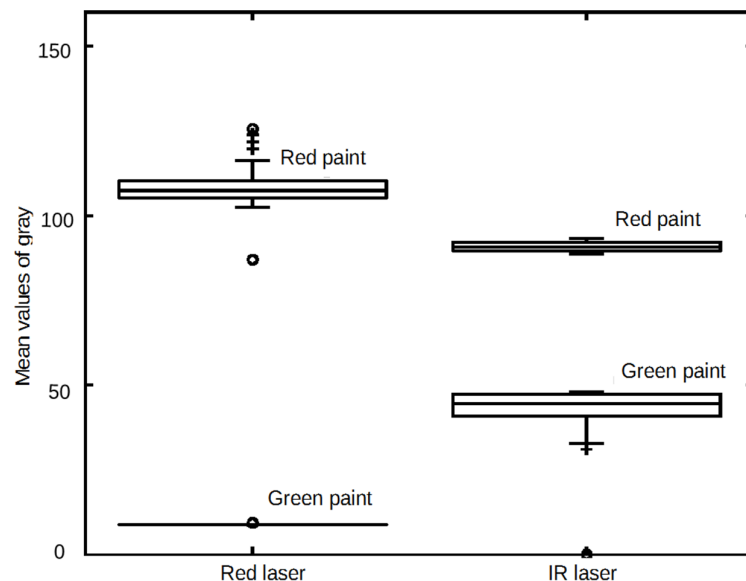


**Figure 4.** Mean values of the light intensity from the speckle histograms of the lasers shinning a red and a green coating in the first five minutes of the drying process.

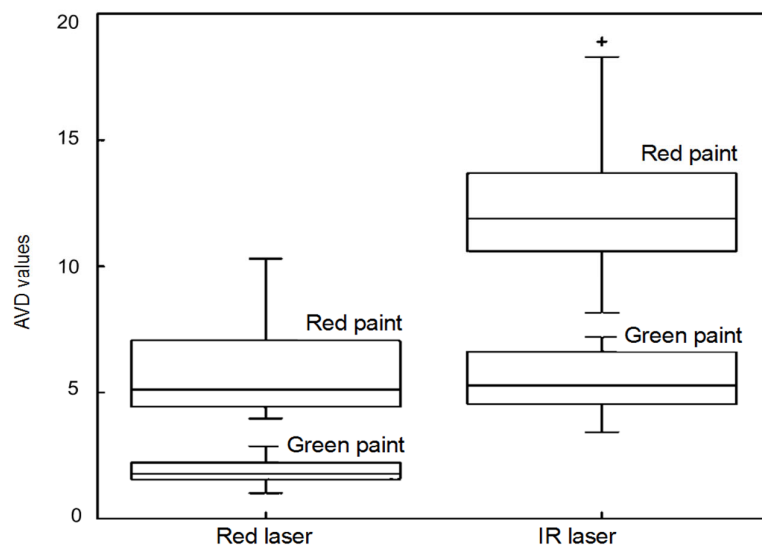


**Figure 5.** DLS measurements of drying paints addressed by the AVD index using red laser and IR laser. Results were obtained the first five minutes after application of the paint.

Accordingly, the reduction of the signal by pigments, such as chlorophyl, can compromise the use of DLS analysis in biological tissues [36–38].

In Figure 4, the boxplot graph presents the distribution of the data, where the box represents the data within the first and third quartiles (25th and 75th, respectively). Meanwhile, the whiskers (minimum and maximum) represent the lower and upper confidence limits, here 1.5 times the interquartile range. The second quartile represents the median value of the data, and it is the line in the box. Points outside of the whiskers are outliers and are represented by (+) or (o).

In Figure 5, we can see the AVD values for both types of lasers in both paints (red and green). When the IR laser was used, the activity measured was higher than when using the

red laser. Thus, the adoption of the IR laser in DLS measurements, despite the influence of the pigment, presented the ability to return a higher signal to be analysed, resulting in higher values of AVD. In addition, the rates between the AVD values of red and green paints were lower when using the IR laser (i.e., a mean of 2.86 for the red laser and of 2.35 for the IR laser).

In Figure 5, the boxplot graph presents the distribution of the data, where the box represents the data within the first and third quartiles (25th and 75th, respectively). Meanwhile, the whiskers (minimum and maximum) represent the lower and upper confidence limits, here 1.5 times the interquartile range. The second quartile represents the median value of the data, and it is the line in the box. Points outside of the whiskers are outliers and are represented by (+) or (o).

The dynamics of the drying process were also recorded (Figure 6). The AVD measurements showed that the values representing the activity from red and IR illumination declined with time due to the volatilization of the solvents taking place during the early stage of the drying process [35]. The AVD measurement obtained from the red wavelength on the red painting presented similarity to the expected profile of a drying paint [11,35]. The low signal observed in the case of the green paint prevented calculations of AVD values (Figure 6).

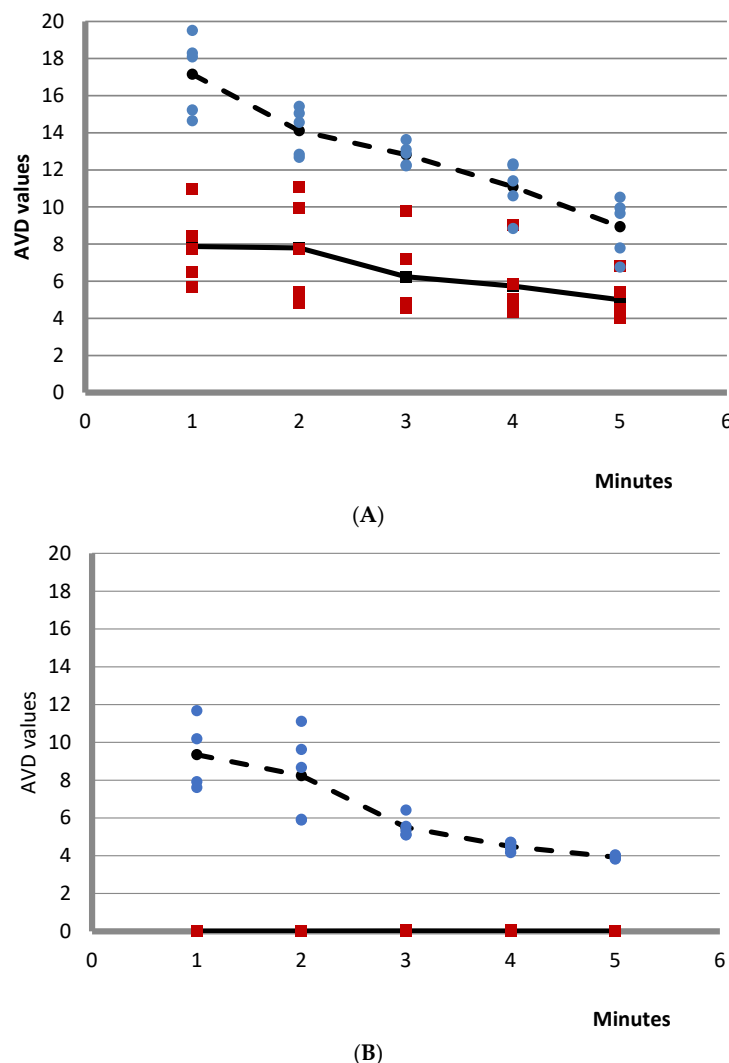


**Figure 6.** AVD values of the red laser and IR laser over time. (A) Drying of the red paint by red laser (red marks) and by IR laser (blue marks). (B) Drying of the green paint using the red laser (red marks) and using the IR laser (blue marks).

In both red and green paints, the calculations of AVD measurements were higher when using IR lasers than when using red lasers. AVD measurements of the green paint were reduced, but a strong signal could be acquired, which demonstrates the reduced absorption of the IR light by red and green pigments and that low absorption did not compromise the DLS patterns and consequently, the AVD.

We observed a strong correlation between the AVD values obtained on the red and green paints using the IR laser (Figure 7). The strong correlation ( $R^2 > 0.9$ ) obtained from DLS indices generated by paints with different reflectance/absorbance showed that the technique can accurately predict the level of water activity in the paint, independently of the pigment nature or content.

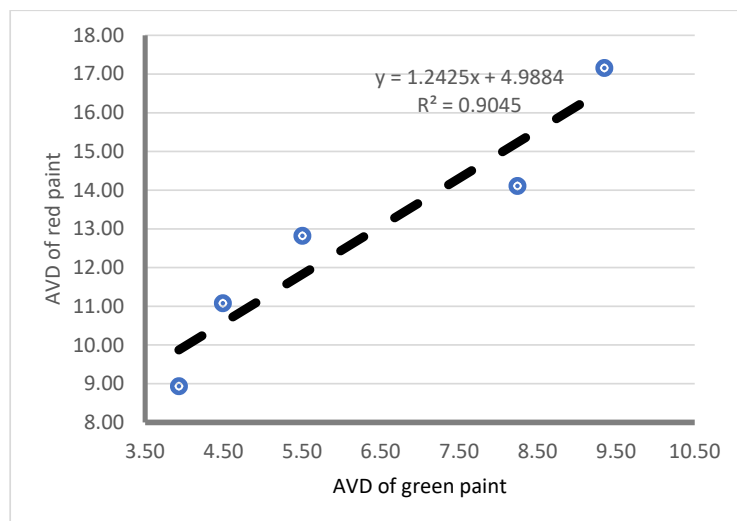


**Figure 7.** Correlation between AVD values of IR laser illumination of green and red paint.

By contrast, in Figure 8, correlations between the DLS signals acquired from red and green paints using the red laser were much reduced. This could indicate that the red laser has different absorption properties for the red and green paints; the DLS analysis obtained from a very low signal in the case of the green paint provided a void result. That could help the understanding of the influence of chlorophyl in DLS outcomes from using red lasers in vegetable tissues [36–38].

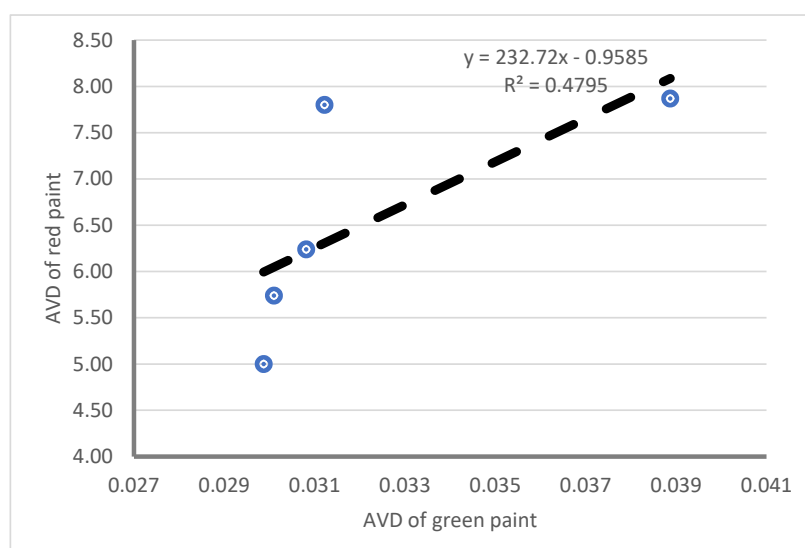


**Figure 8.** Correlation between AVD values of green and red paint using red laser.

### 3.2. Direct Illumination of a Maize Seed Using Red and IR Lasers

The standard deviation (SD) index was used to produce maps of DLS analysis addressing the activity from maize seedlings (Figure 9). When the DLS signal was captured following illumination with the red laser, higher SD index values were obtained (Figure 9A) with strong variations observed across the sample. The radicle showed consistently high SD values, but the seed itself showed the strongest gradients. By comparison, SD values obtained from the IR laser were more consistent across the entire sample (Figure 9B). The radicle showed high SD values, but the seed showed a more constant SD value, as could be expected.

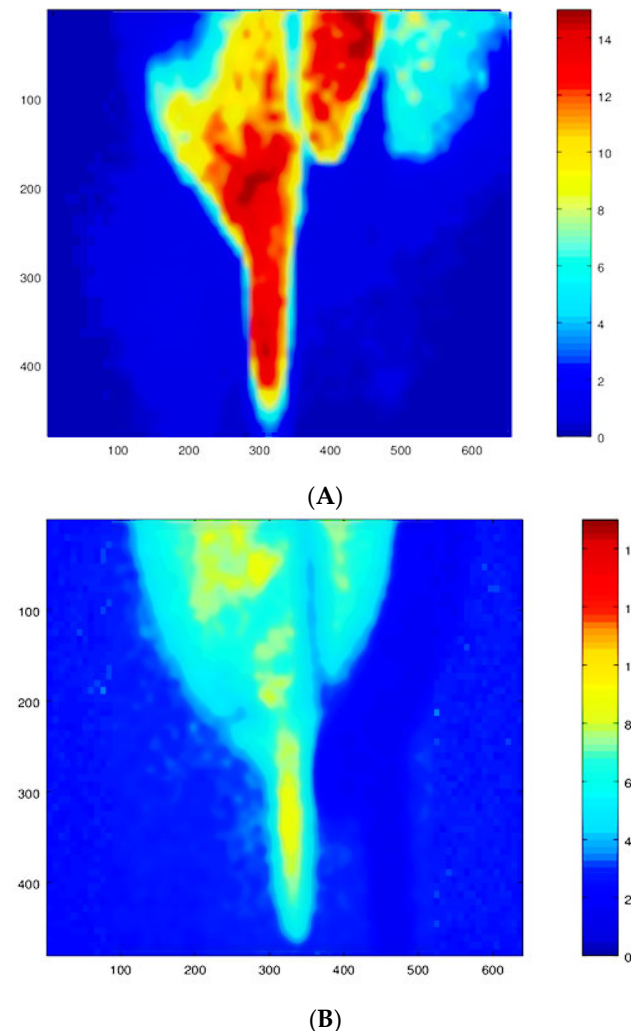


**Figure 9.** Maps of the DLS activity obtained using the SD index on a germinating maize seedling obtained with 660 nm laser illumination and with 780 nm illumination. (A) Typical SD map of a maize seedling obtained using 660 nm laser illumination. (B) Typical SD map of a maize seedling obtained using 780 nm laser illumination. Blue indicates the lowest activity and red the highest activity.

Based on observations made using the paint experiments, we can hypothesise that the high peak SD values and strong gradients observed using red laser illumination were due to the combined reflection, refraction, and scattering of light in the seed–air interface. By contrast, the scattering produced by water is less intense in IR light, with this wavelength absorbed in a higher proportion compared to that with the red laser, as demonstrated in earlier studies [45,46]. The scattering of the IR laser is combined with the scattering produced by the return of the light from the tissue, which is also affected by pigments. That is critical to DLS studies of biological samples because water activity due to evaporation

has an important contribution to the signal recorded [30]. The use of IR light sources to carry out DLS measurements of biological samples could therefore improve computational time since digital filtering may not be needed and online reading of DLS analysis could be achieved.

IR wavelengths are known to be absorbed by water in a greater degree than visible wavelengths. They can also vary in accordance with the range of spectrum the IR is [46]. For example, the higher the IR wavelength is, the higher the absorption will be. Thus, with the wavelength of 780 nm adopted in this work, the absorption is lower than other IR ranges, but the absorption of IR by water is still higher than in the case of red lasers. We did not use high wavelengths of IR in our tests because the absorption would degrade the DLS signal collected. The influence of the water on the results of DLS analysis is relevant [30] since biological samples have water in different bonding and polar clusters [47]; thus, the water activity will influence the DLS outcome, compromising the results when the biological activity is studied. The choice of a suitable IR wavelength is therefore critical to on the one hand reduce the effect of water scattering at the air–sample interface, but also to avoid excessive absorption of the light and excessive reduction of the signal. It is possible, however, that interface processes may be better analysed using visible light lasers than IR lasers.

### 3.3. Use of IR Lasers Improves the Reliability of DLS Measurements in Turbid Medium

The experiment using growing maize seedlings in agar gel analysed both the overall light signal collected from the sample as well as the nature of the DLS measurements extracted. Results showed that the intensity of the light acquired from the tip of the roots (Figure 10) varied drastically between treatments.

In Figure 10, the boxplot graph presents the distribution of the data, where the box represents the data within the first and the third quartiles (25th and 75th, respectively). Meanwhile, the whiskers (minimum and maximum) represent the lower and upper confidence limits, here 1.5 times the interquartile range. The second quartile represents the median value of the data, and it is the line in the box. Points outside of the whiskers are outliers and are represented by (+) or (o).

The dye in the agar gel influenced red laser penetration the most. In the case where illumination occurred with the red laser, the light intensity collected by the camera was reduced by 20% because of the dye (Figure 10A). By comparison, when illumination occurred with the IR laser, we did not observe significant changes in the light intensity because of the dye.

The analysis of the DLS signal, however, gave a different result. Mean AVD values were not affected by the presence of the dye either when the red laser or IR laser were used (Figure 10B). This was expected because the ADV is based on temporal variations of the speckle intensity and its measure is less affected by pixel intensity. However, higher variability of the AVD signal was observed when the red laser was used. This result illustrates how the absorption of the signal reduces the variability of the DLS signal. In the case of the red laser light, absorption is due to the dye and attenuates the intensity of variations in speckle intensity. In the case of IR light, absorption of light is due to water and the variability of the signal is therefore lower than the signal obtained using red light. It is also not affected by the presence of the dye.

The illumination with the IR laser kept the same outcomes in dye and no-dye samples—regarding the level of light intensity, as well as, the AVD values—to biological activity than when red light illumination is used. The increased robustness is particularly evident from the coefficient of variation of the AVD measurements, which were both lower and conserved in the case of IR. The loss of signal due to IR absorption can be overcome using IR lasers with higher power.

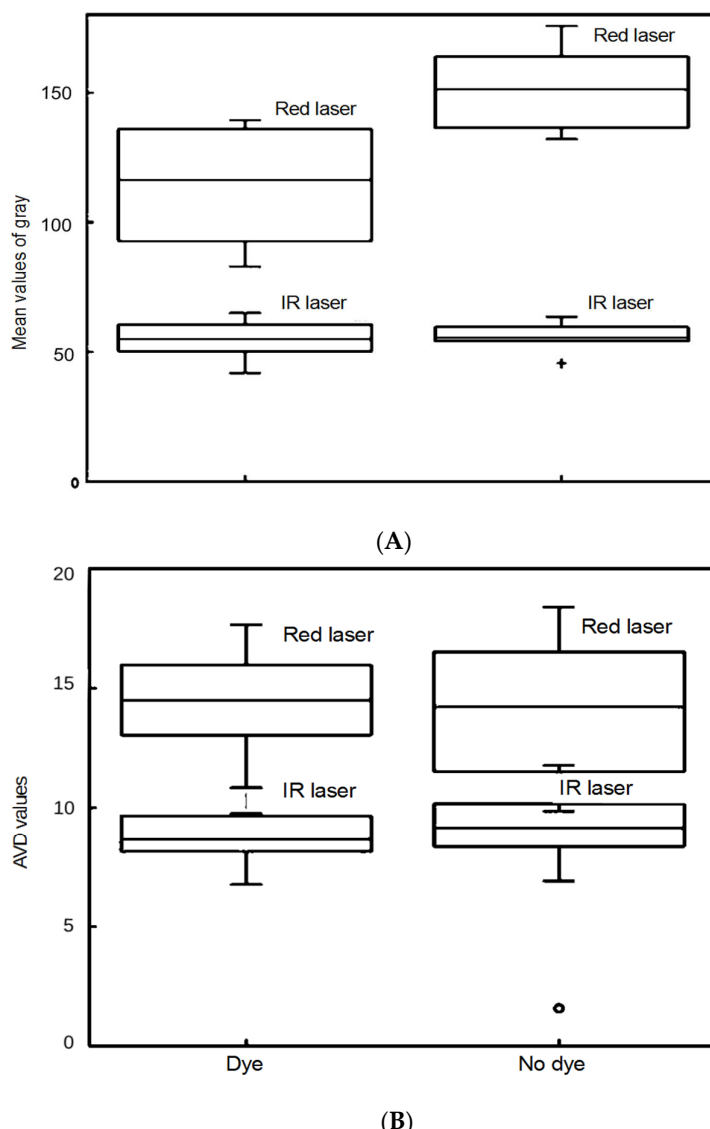


**Figure 10.** Box plot of (A) mean values of light intensity from the speckle histograms and (B) A/D values from the tip of the root inside dye and no-dye gels in a glass tube illuminated by red and IR lasers.

We observed a particular phenomenon comparing the illumination of samples with red and IR lasers. The dispersion of the light was higher when using the red laser than in the case of IR laser illumination. The observed intensity of light by the cameras can be attributed not only to the dispersion, but also by the reflection of light, higher in the red laser. The IR laser penetrates more in the sample, increasing the depolarization, as well as the amount of light returning to the observer (camera) [48]. The IR laser was also more absorbed by water than the red laser.

Finally, the IR laser did not stimulate the vegetable tissues as the visible light from red laser could do [2,49].

The results lead to a potential use of IR lasers in the DLS technique with some advantages with relation to the visible lasers traditionally adopted. In summary, these include the reduction of the variability of the results, the non-influence of the light in the biological tissue, and the reduction of the influence of the pigments on the surface in the DLS results, such as with the case of the chlorophyl. We believe that new studies particularly linked to each application should be carried out to bias the use, and check if the IR laser adoption

presents the advantage claimed. For example, if you need to follow the water activity, the use of an IR laser in DLS analysis can compromise the application.

#### 4. Conclusions

We have compared the dynamical properties of the laser speckles obtained from living biological samples when illuminated by red and IR lasers. Results indicate that even if water absorption limits the quantity of IR light collected by the camera, the analysis of the dynamic laser speckle (DLS) signal is more robust. The dynamics of the speckles generated by IR lasers appeared less sensitive to the turbidity of the environment. Although we could not test the effect of biological pigments, experiments carried out with paints indicate that the DLS phenomenon produced by IR lasers is less sensitive to pigments, too. Using analogy, that fact can lead us to reinforce the advantage of the IR laser in DLS analysis when chlorophyl is present if compared to visible lasers. Finally, we proved that the penetration of IR lasers offers an additional feature to its use regarding the ability to bring more information from within. Hence, results in this study suggest that the use of IR lasers to carry out DLS analysis of biological samples could greatly enhance the robustness of measured acquired.

**Author Contributions:** Conceptualization, L.X.D. and R.A.B.J.; consultancy in biology and review, M.P. and J.D.; writing—review and editing, R.J.G.-P. and R.A.B.J.; conduction of the assays, image processing, writing, E.W.N.C.; consultancy in biospeckle laser, R.A.B.J.; consultancy in physics, R.J.G.-P.; supplementary assays, R.J.G.-P. All authors have read and agreed to the published version of the manuscript.

**Funding:** CAPES scholarship PNPD Program, FAPEMIG (CAG PPM 163/17), and CNPQ (PQ 306692/2016-30).

**Institutional Review Board Statement:** Not applicable.

**Informed Consent Statement:** Not applicable.

**Data Availability Statement:** Data from this study are not publicly available.

**Acknowledgments:** We wish to acknowledge the partial financial support for this study provided by the CAPES scholarship PNPD Program, FAPEMIG (CAG PPM 163/17), and CNPQ (PQ 306692/2016-30).

**Conflicts of Interest:** The authors declare no conflict of interest.

#### References

1. Nadimi, M.; Sun, D.-W.; Paliwal, J. Recent applications of novel laser techniques for enhancing agricultural production. *Laser Phys.* **2021**, *31*, 053001. [[CrossRef](#)]
2. Hernandez, A.C.; Dominguez, P.A.; Cruz, O.A.; Ivanov, R.; Carballo, C.A.; Zepeda, B.R. Laser in agriculture. *Int. Agrophys.* **2010**, *24*, 407–422.
3. Gebbers, R.; Adamchuk, V.I. Precision agriculture and food security. *Science* **2010**, *327*, 828–831. [[CrossRef](#)] [[PubMed](#)]
4. Fennimore, S.A.; Slaughter, D.C.; Siemens, M.C.; Leon, R.G.; Saber, M.N. Technology for Automation of Weed Control in Specialty Crops. *Weed Technol.* **2016**, *30*, 823–837. [[CrossRef](#)]
5. Mohammed, G.H.; Colombo, R.; Middleton, E.M.; Rascher, U.; van der Tol, C.; Nedbal, L.; Goulas, Y.; Pérez-Priego, O.; Damm, A.; Meroni, M.; et al. Remote sensing of solar-induced chlorophyll fluorescence (SIF) in vegetation: 50 years of progress. *Remote Sens. Environ.* **2019**, *231*, 111177. [[CrossRef](#)]
6. Eyre, R.; Lindsay, J.; Laamrani, A.; Berg, A. Within-Field Yield Prediction in Cereal Crops Using LiDAR-Derived Topographic Attributes with Geographically Weighted Regression Models. *Remote Sens.* **2021**, *13*, 4152. [[CrossRef](#)]
7. Weiss, U.; Biber, P. Plant detection and mapping for agricultural robots using a 3D LIDAR sensor. *Robot. Auton. Syst.* **2011**, *59*, 265–273. [[CrossRef](#)]
8. Cheng, Y.; Wang, G.Y. Mobile robot navigation based on lidar. In Proceedings of the 2018 Chinese Control and Decision Conference (CCDC), Shenyang, China, 9–11 June 2018; pp. 1243–1246.
9. Mei, L.; Guan, Z.G.; Zhou, H.J.; Lv, J.; Zhu, Z.R.; Cheng, J.A.; Chen, F.J.; Löfstedt, C.; Svanberg, S.; Somesfalean, G. Agricultural pest monitoring using fluorescence lidar techniques. *Appl. Phys. B Laser Opt.* **2011**, *106*, 733–740. [[CrossRef](#)]
10. Murphy, P.N.C.; Ogilvie, J.; Arp, P. Topographic modelling of soil moisture conditions: A comparison and verification of two models. *Eur. J. Soil Sci.* **2009**, *60*, 94–109. [[CrossRef](#)]

11. Amalvy, J.I.; Lasquibar, C.A.; Arizaga, R.; Rabal, H.; Trivi, M. Application of dynamic speckle interferometry to the drying of coatings. *Prog. Org. Coat.* **2001**, *42*, 89–99. [[CrossRef](#)]
12. Langevin, D.; Lozano, O.; Salvati, A.; Kestens, V.; Monopoli, M.; Raspaud, E.; Mariot, S.; Salonen, A.; Thomas, S.; Driessen, M.; et al. Inter-laboratory comparison of nanoparticle size measurements using dynamic light scattering and differential centrifugal sedimentation. *Nanoimpact* **2018**, *10*, 97–107. [[CrossRef](#)]
13. Fujii, H.; Asakura, T.; Nohira, K.; Shintomi, Y.; Ohura, T. Blood flow observed by time-varying laser speckle. *Opt. Lett.* **1985**, *10*, 104–106. [[CrossRef](#)]
14. Dunn, A.K.; Devor, A.; Bolay, H.; Andermann, M.L.; Moskowitz, M.A.; Dale, A.M.; Boas, D.A. Simultaneous imaging of total cerebral hemoglobin concentration, oxygenation, and blood flow during functional activation. *Opt. Lett.* **2003**, *28*, 28–30. [[CrossRef](#)]
15. Xu, Z.; Joenathan, C.; Khorana, B.M. Temporal and spatial properties of the time-varying speckles of botanical specimens. *Opt. Eng.* **1995**, *34*, 1487–1502. [[CrossRef](#)]
16. Zdunek, A.; Adamiak, A.; Pieczywek, P.M.; Kurenda, A. The biospeckle method for the investigation of agricultural crops: A review. *Opt. Lasers Eng.* **2014**, *52*, 276–285. [[CrossRef](#)]
17. Braga, R.A.; Fabbro, I.M.D.; Borem, F.M.; Rabelo, G.; Arizaga, R.; Rabal, H.J.; Trivi, M. Assessment of Seed Viability by Laser Speckle Techniques. *Biosyst. Eng.* **2003**, *86*, 287–294. [[CrossRef](#)]
18. Vivas, P.; Resende, L.; Braga, R.; Guimarães, R.; Azevedo, R.; da Silva, E.; Toorop, P. Biospeckle activity in coffee seeds is associated non-destructively with seedling quality. *Ann. Appl. Biol.* **2016**, *170*, 141–149. [[CrossRef](#)]
19. Singh, P.; Chatterjee, A.; Rajput, L.S.; Rana, S.; Kumar, S.; Nataraj, V.; Bhatia, V.; Prakash, S. Development of an intelligent laser biospeckle system for early detection and classification of soybean seeds infected with seed-borne fungal pathogen (*Colletotrichum truncatum*). *Biosyst. Eng.* **2021**, *212*, 442–457. [[CrossRef](#)]
20. Ribeiro, K.M.; Barreto, B.; Pasqual, M.; White, P.J.; Braga, R.A.; Dupuy, L.X. Continuous, high-resolution biospeckle imaging reveals a discrete zone of activity at the root apex that responds to contact with obstacles. *Ann. Bot.* **2013**, *113*, 555–563. [[CrossRef](#)]
21. Kurenda, A.; Adamiak, A.; Zdunek, A. Temperature effect on apple biospeckle activity evaluated with different indices. *Postharvest Biol. Technol.* **2012**, *67*, 118–123. [[CrossRef](#)]
22. Rezende, R.A.L.S.; Soares, J.D.R.; Dos Santos, H.O.; Pasqual, M.; Junior, R.A.B.; Reis, R.O.; Rodrigues, F.A. Effects of silicon on antioxidant enzymes, CO<sub>2</sub>, proline and biological activity of in vitro-grown cape gooseberry under salinity stress. *Aust. J. Crop Sci.* **2017**, *11*, 438–446. [[CrossRef](#)]
23. Pajuelo, M.; Baldwin, G.E.; Rabal, H.; Cap, N.; Arizaga, R.; Trivi, M. Bio-speckle assessment of bruising in fruits. *Opt. Lasers Eng.* **2003**, *40*, 13–24. [[CrossRef](#)]
24. Amaral, I.C.; Braga, R.A.; Ramos, E.M.; Ramos, A.L.S.; Roxael, E.A.R. Application of biospeckle laser technique for determining biological phenomena related to beef aging. *J. Food Eng.* **2013**, *119*, 135–139. [[CrossRef](#)]
25. Pomarico, J.A.; DiRocco, H.O. Compact device for assessment of microorganism motility. *Rev. Sci. Instrum.* **2004**, *75*, 4727–4731. [[CrossRef](#)]
26. Tuchin, V.V. Tissue Optics and Photonics: Biological Tissue Structures. *J. Biomed. Photon Eng.* **2015**, *1*, 3–21. [[CrossRef](#)]
27. Tuchin, V.V. Tissue Optics and Photonics: Light-Tissue Interaction. *J. Biomed. Photon Eng.* **2015**, *1*, 98–134. [[CrossRef](#)]
28. Carvalho, P.H.; Barreto, J.B.; Braga, R.A.; Rabelo, G.F. Motility parameters assessment of bovine frozen semen by biospeckle laser (BSL) system. *Biosyst. Eng.* **2009**, *102*, 31–35. [[CrossRef](#)]
29. Reis, R.O.; Rabal, H.J.; Braga, R.A. Light intensity independence during dynamic laser speckle analysis. *Opt. Commun.* **2016**, *366*, 185–193. [[CrossRef](#)]
30. Cardoso, R.R.; Costa, A.G.; Nobre, C.M.B.; Braga, R.A. Frequency signature of water activity by biospeckle laser. *Opt. Commun.* **2011**, *284*, 2131–2136. [[CrossRef](#)]
31. Lammertyn, J.; Peirs, A.; De Baerdemaeker, J.; Nicolaï, B. Light penetration properties of NIR radiation in fruit with respect to non-destructive quality assessment. *Postharvest Biol. Technol.* **2000**, *18*, 121–132. [[CrossRef](#)]
32. Alves, J.A.; Braga, R.A.; Boas, E.V.D.B.V. Identification of respiration rate and water activity change in fresh-cut carrots using biospeckle laser and frequency approach. *Postharvest Biol. Technol.* **2013**, *86*, 381–386. [[CrossRef](#)]
33. Cover, T.M.; Thomas, J.A. *Elements of Information Theory*; John Wiley and Sons: Hoboken, NJ, USA, 2005.
34. Brunel, L.; Brun, A.; Snabre, P. Microstructure movements study by dynamic speckle analysis. *Speckle06 Speckles Grains Flowers* **2006**, *6341*, 475–480. [[CrossRef](#)]
35. Pérez, A.J.; González-Peña, R.J.; Braga, R., Jr.; Perles, Á.; Pérez-Marín, E.; García-Diego, F.J. A Portable Dynamic Laser Speckle System for Sensing Long-Term Changes Caused by Treatments in Painting Conservation. *Sensors* **2018**, *18*, 190. [[CrossRef](#)]
36. Nader, C.A.; Tualle, J.-M.; Tinet, E.; Ettori, D. A New Insight into Biospeckle Activity in Apple Tissues. *Sensors* **2019**, *19*, 497. [[CrossRef](#)]
37. Arefi, A.; Moghaddam, P.A.; Motlagh, A.M.; Hassanpour, A. Towards real-time speckle image processing for mealiness assessment in apple fruit. *Int. J. Food Prop.* **2017**, *20*, S3135–S3148. [[CrossRef](#)]
38. Pieczywek, P.M.; Nowacka, M.; Dadan, M.; Wiktor, A.; Rybak, K.; Witrowa-Rajchert, D.; Zdunek, A. Postharvest Monitoring of Tomato Ripening Using the Dynamic Laser Speckle. *Sensors* **2018**, *18*, 1093. [[CrossRef](#)]
39. Godinho, R.; Silva, M.; Nozela, J.; Braga, R. Online biospeckle assessment without loss of definition and resolution by motion history image. *Opt. Lasers Eng.* **2012**, *50*, 366–372. [[CrossRef](#)]

40. Ansari, M.Z.; Ramírez-Miquet, E.E.; Otero, I.; Rodríguez, D.; Darias, J.G. Real time and online dynamic speckle assessment of growing bacteria using the method of motion history image. *J. Biomed. Opt.* **2016**, *21*, 66006. [[CrossRef](#)]
41. Rivera, F.P.; Braga, R.A. Bio-Speckle Laser Tool Library. Available online: <https://www.nongnu.org/bsl1/> (accessed on 22 February 2023).
42. Blotta, E.; Ballarín, V.; Brun, M.; Rabal, H. Evaluation of speckle-interferometry descriptors to measuring drying-of-coatings. *Signal Process.* **2011**, *91*, 2395–2403. [[CrossRef](#)]
43. Braga Júnior, R.A.; Rivera, F.P.; Moreira, J. *A Practical Guide to Biospeckle Laser Analysis: Theory and Software*; UFLA: Lavras, Brazil, 2016.
44. Braga, R.; Nobre, C.; Costa, A.; Sáfadi, T.; da Costa, F. Evaluation of activity through dynamic laser speckle using the absolute value of the differences. *Opt. Commun.* **2011**, *284*, 646–650. [[CrossRef](#)]
45. Cios, A.; Ciepielak, M.; Szymański, Ł.; Lewicka, A.; Cierniak, S.; Stankiewicz, W.; Mendrycka, M.; Lewicki, S. Effect of Different Wavelengths of Laser Irradiation on the Skin Cells. *Int. J. Mol. Sci.* **2021**, *22*, 2437. [[CrossRef](#)] [[PubMed](#)]
46. Gordon, I.E.; Rothman, L.S.; Gamache, R.R.; Jacquemart, D.; Boone, C.; Bernath, P.F.; Shephard, M.W.; Delamere, J.S.; Clough, S.A. Current updates of the water-vapor line list in HITRAN: A new “Diet” for air-broadened half-widths. *J. Quant. Spectrosc. Radiat. Transf.* **2007**, *108*, 389–402. [[CrossRef](#)]
47. Braga, R.A.; Rabelo, G.F.; Barreto Filho, J.B.; Borem, F.M.; Pereira, J.; Muramatsu, M.; Dal Frabbro, I.M. Chapter 8. Applications in Biological Samples. In *Dynamic Laser Speckle and Applications*; Rabal, H., Braga, R.A., Eds.; CRC Press: Boca Raton, FL, USA, 2008; pp. 194–195.
48. Ryckewaert, M.; Héran, D.; Faur, E.; George, P.; Grèzes-Besset, B.; Chazallet, F.; Abautret, Y.; Zerrad, M.; Amra, C.; Bendoula, R. A New Optical Sensor Based on Laser Speckle and Chemometrics for Precision Agriculture: Application to Sunflower Plant-Breeding. *Sensors* **2020**, *20*, 4652. [[CrossRef](#)] [[PubMed](#)]
49. Burbach, C.; Markus, K.; Zhang, Y.; Schlicht, M.; Baluška, F. Photophobic behavior of maize roots. *Plant Signal. Behav.* **2012**, *7*, 874–878. [[CrossRef](#)] [[PubMed](#)]

**Disclaimer/Publisher’s Note:** The statements, opinions and data contained in all publications are solely those of the individual author(s) and contributor(s) and not of MDPI and/or the editor(s). MDPI and/or the editor(s) disclaim responsibility for any injury to people or property resulting from any ideas, methods, instructions or products referred to in the content.